Collimator Selection for SPECT Brain Imaging: The Advantage of High Resolution

Stefan P. Mueller, Joseph F. Polak, Marie Foley Kijewski, and B. Leonard Holman

Department of Radiology, Harvard Medical School, and Brigham and Women's Hospital, Boston, Massachusetts

We compared a prototype long-bore (LB) high-resolution collimator with a low-energy, general-purpose collimator (LEGP) using ^{99m}Tc and ^{123}I. The LB collimator provided a 56% improvement in tomographic resolution (autocorrelation width) over the LEGP for ^{99m}Tc; for ^{123}I, the gain was 79%, providing substantially improved contrast for small structures. The sensitivity of the LB collimator, however, is only 32% of that of the LEGP. The imaging tasks to be performed on [^{123}I]IMP brain scans involve localization and discrimination of small, high-contrast brain structures and detection of abnormalities in shape, size, or uptake, rather than simple detection of lesions. Observer performance in such higher-order imaging tasks is known to depend on high spatial resolution, even at the cost of sensitivity. Patient studies confirmed that, for resolution-limited tasks, the increase in resolution outweighs the increased noise due to a loss in sensitivity. When the tomographic resolution of the LB collimator was degraded by smoothing to that of the LEGP, the noise in the LB images was lower than that of the LEGP by a factor of 2.9 for the same imaging time, demonstrating the advantage of high-resolution detectors and a smooth reconstruction filter over low-resolution detectors without smoothing. Therefore, collimators designed for high resolution, even at substantial cost in sensitivity, are expected to yield significant improvements for brain SPECT. Geometric calculations show that commercially available low-energy, high-resolution cast collimators promise to meet these requirements.

Functional brain imaging with single photon emission computed tomography (SPECT) and iodine-123 (^{123}I) and technetium-99m- (^{99m}Tc) labeled amines has recently been applied to cerebrovascular disease, stroke, dementia, and epilepsy (*1–3*). Because spatial resolution is degraded owing to the 2% abundance of high-energy photons from ^{123}I itself, and from ^{124}I when ^{123}I is produced by the Te(p,2n)^{123}I reaction, optimal collimation for ^{123}I imaging has received much attention (*4–10*). In this report, we address collimator selection for SPECT with ^{123}I and ^{99m}Tc, taking into account the trade-off between sensitivity and resolution and its effects on image quality.

Observer performance is often predicted by the signal to noise ratio (SNR) for detection tasks. This approach has been widely used with transmission computed tomography (TCT), where the objects of interest have low contrast and are large with respect to system resolution (*11–13*). For these large, low-contrast objects, detectability depends primarily on the image noise (*13*). Expressions for the root mean square error (%RMS) in a pixel or region of interest have been derived to characterize emission computed tomography (ECT) systems (*14–16*). Unlike TCT, however, the structures of interest in brain ECT are high-contrast features which are small compared with the system resolution (*17*). High resolution is required to preserve the object contrast in the image. The influence of resolution and object shape and size on radionuclide quantitation has been studied extensively for ECT (*17–19*), but the effects of the image noise have been neglected. The trade-off between increased measurement accuracy due to improved resolution and, consequently, higher contrast recovery and a loss in precision due to decreased sensitivity is an important issue.

The diagnostic tasks to be performed with SPECT studies of the brain require localization and identification of cortical and ganglional structures and the recognition of abnormalities in shape, size, or uptake.

These tasks are made more difficult by the complex nonuniform background in which the structures of interest are imbedded. Such higher-order tasks pose different requirements for the imaging system than does simple detection of low contrast features in a uniform background. Hanson has derived the SNR, a measure of performance, for such tasks (20). He found that for localization, sizing, and object separation, optimal performance requires more high spatial frequency information than for detection, even with a uniform background. Furthermore, he demonstrated that a nonuniform background reduces the importance of low spatial frequency information. These predictions are supported by a recent simulation study by Muehllehner, demonstrating that the number of counts required for a given SNR decreases with increasing resolution for higher-order tasks such as separation of high-contrast bars or rods (21).

With ECT, system resolution or bandwidth is determined not only by the physical aperture, but also by the apodization window used in the reconstruction algorithm. When two ECT systems with equal bandwidth and sensitivity are compared, the SNR of the system with high resolution detectors and a "smooth" reconstruction filter is superior to one with lower detector resolution and a "sharp" reconstruction (11,12). This principle, called signal amplification technique (SAT) by Phelps (22), is an important design consideration for positron emission tomography systems and will also affect our assessment of collimator performance.

In the present study, we investigated the tradeoff between sensitivity and resolution for brain SPECT with a rotating camera by comparing a prototype long-bore foil collimator (LB) described by Palmer et al. (23) with the low-energy, general-purpose cast collimator (LEGP).* The comparison was made in terms of signal passband and %RMS noise transferred through the entire system. This analysis allowed us to evaluate the effect of collimator penetration on image quality using [123]I. In the second part of our analysis, we evaluated the performance of other collimators using the geometric collimator design equations and extrapolations based on our experimental study.

METHODS

Definitions

The signal contribution in an image is the convolution of the system line spread function (LSF) with the object function. This relationship can be expressed in the frequency domain as the product of the modulation-transfer function (MTF) and the Fourier transform of the object.

A figure of merit for system resolution is the equiv-alent passband; this quantity, which can be expressed as the integral of the squared MTF, represents the total signal power in the image for an object with a white power spectrum. Systems with the same equivalent passband transfer the same noise power if the input noise power spectrum is white. The reciprocal of this integral has the dimension of length, and defines an aperture or resolution width, which can be interpreted as a noise-equivalent aperture (12). Its interpretation in the spatial domain is the mean distance of uncorrelated points in the image; the quantity is therefore often called the autocorrelation width (ACW) (24).

$$ACW = \left[\int\limits_0^\infty MTF^2(f) \, df \right]^{-1}.$$

The ACW is related to the information content (information bandwidth integral) (13) and the visual impression of sharpness of an image (acutance) (12). Hence, ACW is among the most comprehensive single measures of spatial resolution. The more familiar full width half maximum (FWHM) parameter describes frequency transfer properties only for Gaussian LSFs, which often do not characterize real systems with scatter and penetration (25,26). The FWHM is reported here only for comparative purposes and for geometrical collimator calculations.

Noise is measured for a uniform source which is large compared to the system aperture. The total noise power is given by the variance (s^2) in the image. The pixel root mean square error (%RMS) is the ratio of the standard deviation (s) and the mean counts ($\bar{x}$) in the image:

$$\%RMS = 100 \, s/\bar{x}.$$

The %RMS resembles the standard error, which is related to the precision of a measurement, but does not describe the accuracy of radionuclide quantitation in objects close to the size of the system aperture.

Geometrical calculations

The FWHM resolution (r) at distance b from the front surface of a parallel hole collimator with hole diameter (d), collimator thickness (a), and a given distance from the back surface of the collimator to the mean interaction depth in the camera crystal c is:

$$R = d/ae \cdot (a + b + c),$$

where ae = a −2/my, describes the effective hole length given edge penetration (27,28). The collimator efficiency (E) depends on the septal thickness (s), and the efficiency k for a given hole shape (27):

$$E = [k \cdot d/ae \cdot d/(d + s)]^2.$$

These geometric parameters, however, do not completely characterize the image quality in the presence of scatter and collimator penetration. The influence of

scatter on the image contrast is independent of the collimator (25) and, therefore, cancels out for the comparison of contrast ratios scanning the same source. The contrast degradation due to collimator penetration, however, commonly characterized by the shortest path-length for penetrating radiation (w) (27):

$$w = a \cdot s/(2d + s),$$

and, for a given linear attenuation coefficient (μ_1) for the collimator material

$$P < \exp(-\mu_1 \cdot w).$$

Contrast degradation due to penetration (D_{pen}) can formally be treated similarly to scatter and, thus, D_{pen} = 1/(1 + PF), where PF is the penetration fraction (the ratio of the accepted penetrating photons to the total number of accepted photons). For a point source, the penetration fraction is a function of collimator penetration and imaging distance, since the solid angle for penetrating photons decreases with increasing imaging distance while the geometric sensitivity of the collimator is independent of the imaging distance. To simplify our analysis we, therefore, compared collimators with lower penetration than our reference, the LEGP collimator, and used the same imaging distance of 17 cm, although some collimators cannot be used for brain imaging at that radius of rotation.

We can describe the image contrast in terms of the contrast reduction due to limited resolution which is a function of the system point-spread function (PSF) and size and shape of the object. Assuming a Gaussian PSF with an FWHM of R, the contrast (C) in the center of a spherical object of diameter diam is:

$$C = 2 \cdot [\text{erf(sig)} - \text{sig}(2\pi)^{-\frac{1}{2}} \exp(-0.5 \cdot \text{sig}^2],$$

where sig = diam/(0.424661·R) (the contrast converts from FWHM to sigma for the Gaussian PSF) and erf (sig) is the integral from 0 to sig of a Gaussian with a sigma and an area of 1.

Data acquisition

A large field-of-view rotating gamma camera[†] with energy and linearity correction hardware was used for all measurements. The symmetric pulse-height-analyzer windows were 126-154 keV for ^{99m}Tc, and 144-176 keV for [123]I. We compared the standard low-energy-general-purpose (LEGP) collimator with the long-bore (LB) collimator (Table 1) described by Palmer et al. (23). Radii of rotation were measured from the outer collimator surface to the center-of-rotation. Data were acquired in 64 × 64 or 128 × 128 matrices, corresponding to pixels of 0.63 or 0.31 cm. Measurements were made using [^{99m}Tc]pertechnetate or N-isopropyl-^{123}I-p-iodoamphetamine[‡] (4-5% [124]I contamination).

Phantom studies

Tomographic LSFs were measured using a polyethylene tube of inner diameter 0.58 mm, filled with either 4 mCi of [^{99m}Tc]pertechnetate or 2 mCi of [^{123}I]iodoamphetamine (IMP), suspended in the center of a water-filled 20-cm diameter cylindrical phantom. We acquired 128 projections in a 128 × 128 matrix for both collimators at radii of rotation of 17 and 22 cm. No attenuation correction was applied.

For noise measurements, a 20-cm-diameter cylindrical phantom was filled with an average ^{123}I concentration of 1 μCi/ml, corresponding to the average concentration of [^{123}I]IMP in the brain. We acquired 64 projections in a 64 × 64 matrix at acquisition times of 1, 2, 3, 4, 5, 7, 10, 15, 30, 45, and 90 sec/projection at

TABLE 1
Collimator Characteristics[*]

	LEGP	LB	LEHR	ME
Collimator thickness [cm]	4.10	13.0	4.00	4.15
Hole diameter [mm]	2.50	4.40	1.80	3.40
Septal thickness [mm]	0.30	0.18	0.30	1.40
System resolution [cm]	1.41	1.11	1.07	1.87
Relative efficiency	1.00	0.34	0.50	1.14
Max. penetration [%]	0.94	0.53	0.20	0.00
Relative contrast				
0.5 cm sphere	1.00	1.98	2.22	0.44
1.0 cm sphere	1.00	1.81	1.99	0.47
2.0 cm sphere	1.00	1.37	1.43	0.59
3.0 cm sphere	1.00	1.09	1.10	0.76

[*] Physical parameters and performance characteristics based on geometric calculations for 160 keV photons. All collimators have hexagonal holes. LB collimator is made of foil; all others are cast collimators. System resolution for intrinsic resolution of 3.8 mm was calculated at imaging distance of 17 cm from collimator surface. Contrast is given relative to contrast of LEGP collimator. Because of higher penetration, contrast for LEGP collimator is expected to be less than calculated; conversely, contrast for LB, LEHR, and ME collimators is expected to be better than predicted.

radii of rotation of 22 cm for the LEGP and 17 cm for the LB collimator. Mean ($\bar{x}$) and standard deviation (s) were calculated in the reconstruction from a circular region with 80% of the phantom's diameter. The %RMS noise as a function of total image counts (N_{tot}) is proportional to $(N_{tot})^{-\frac{1}{2}}$ for a large uniform source (14-16). We, therefore, fitted our data using a linear least squares model to the logarithmic transform of:

$$\%RMS = k \cdot (N_{tot})^{-\frac{1}{2}}$$

to obtain k, a parameter of the system noise amplification.

Simulations

To study the tomographic point response in the presence of scatter and penetration in the projections we simulated projection data of a line source with monoexponential tails, representing scatter (29,30), superimposed on a constant background, representing penetration (Fig. 1). The simulated line source contains all features of the line response measured in the phantom (Fig. 2); these projection data were reconstructed by filtered backprojection.

Image Reconstruction and Data Processing

We acquired a 60-million-count image of a refillable sheet source for uniformity correction (31). The effective attenuation coefficient (μ) for the first-order hyperbolic sine correction (32) was determined by the following procedure: second-order radially symmetric polynomial surfaces were fitted to groups of five reconstructed slices through a cylindrical phantom, and the
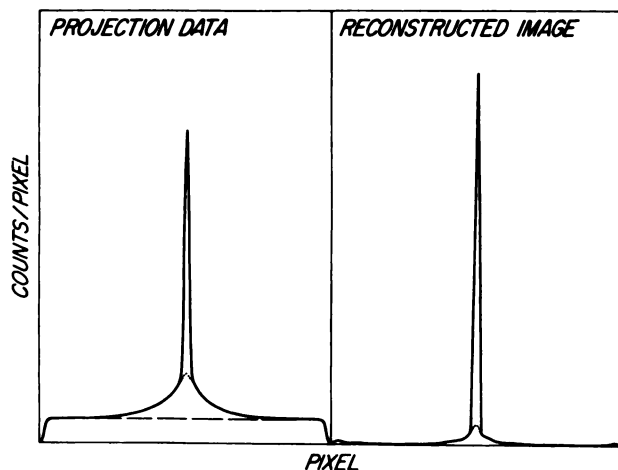

FIGURE 1
Line spread functions for ^{123}I and ^{99m}Tc line sources imaged at center of 20-cm-diameter water-filled phantom are displayed on semi-logarithmic scale. 17-cm outer-collimator-surface-to-line-source distance was used. Both curves are normalized to their maxima. Plateau on ^{123}I curve is due to penetration of high-energy photons of both ^{123}I and ^{124}I contaminant
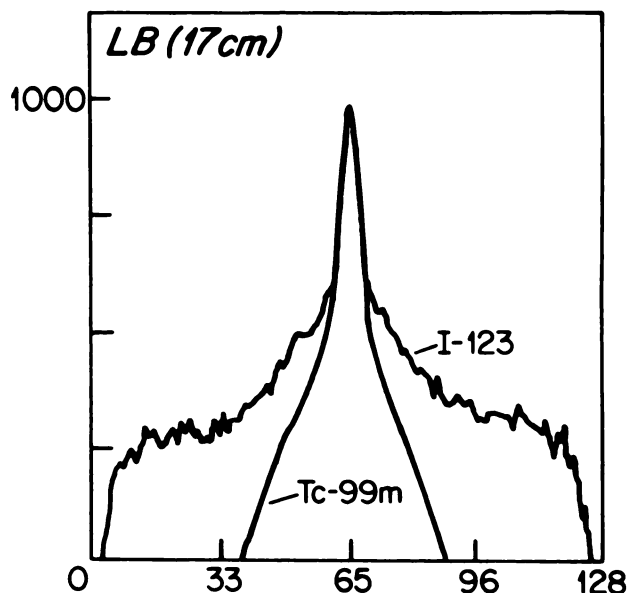

FIGURE 2
Tomographic point spread function (PSF) in presence of scatter and penetration differs from PSF in projections. Contribution from exponential scatter tails, although reduced, degrades contrast in tomographic image. Constant background from penetration, on the other hand, is back-projected into ring around field-of-view and has minimal influence on contrast

best μ determined by iteration yielding a zero value for the quadratic term of the fit.

We used a filtered backprojection algorithm for all reconstructions. Hanning windows with a cutoff frequency of 0.8 cm^{-1} were used as apodization filters; the cutoff frequency corresponds to Nyquist sampling in the 64 × 64 acquisition currently used for clinical applications. These were compared with images reconstructed without apodization. Noise measurements and clinical studies were also investigated after applying a three-dimensional Hanning apodization window (cutoff 0.8 cm^{-1}) to images reconstructed with a ramp filtered backprojection. This filter yields the same apodization within the slice as a one-dimensional Hanning window with the same cutoff frequency applied to the projections. In addition, the same filter kernel was applied between slices, resulting in a more isotropic point response.

We obtained line-spread functions as five-pixel-wide profiles through the line-source images in the projections, and as one-pixel-wide horizontal profiles through the maximum value in the tomographic reconstruction. The maximum of the LSF was estimated from a paraboloid through the three highest data points, and the FWHM was calculated by linear interpolation. MTFs were computed as the magnitude of the discrete Fourier transform of the LSF. The reported FWHM and ACW values represented the mean of ten measurements for ^{99m}Tc and five for ^{123}I.

Patient studies

To determine whether the differences in performance between the LB and LEGP collimators observed in phantom studies could be observed in the clinical realm, we studied five patients with neurological disease (four with cerebrovascular disorders and one with multiple sclerosis).

SPECT imaging began 15 min after the i.v. injection of 5 mCi [^{123}I]IMP. Sixty-four angular projections were collected over 360° at 25 sec to 40 sec per projection. Pixel dimension and slice thickness were each 6.3 mm. A three-dimensional Hanning window with cutoff frequency of 0.8 cm^{-1} was applied to the data during reconstruction. Horizontal profiles through the reconstructions were used to assess image contrast. Three observers, unaware of the technical and clinical data, reviewed the two transaxial data sets for each patient and scored image quality on a three-point scale: LB worse than LEGP, LB equal to LEGP, or LB better than LEGP.

RESULTS

Planar resolution

The spatial resolution in the projection data for imaging ^{99m}Tc at 17 cm radius of rotation was 1.19 ± 0.06 cm FWHM and 3.41 ± 0.11 cm ACW for the LB collimator and 1.69 ± 0.06 cm FWHM and 4.23 ± 0.20 cm ACW for the LEGP. The LEGP MTF completely rolled off at a frequency of 0.74 cm^{-1}. The LB collimator had a higher bandwidth, but no significant signal power was found beyond 0.8 cm^{-1}, the Nyquist frequency for acquisitions in a 64 × 64 matrix.

We compared the projection LSF for ^{99m}Tc and ^{123}I for the LB collimator at 17 cm (Fig. 1). The geometric peaks were similar; however, there were increased tails primarily from scatter and an almost constant background due to penetration seen for ^{123}I.

Simulations

The image reconstructed from the projection data simulating a line source with scatter and penetration demonstrates the relative importance of these two components on image contrast (Fig. 2). The constant background in the projections contributed to the reconstructed image mainly along the edge of the field-of-view. The effects of this background on image contrast will be minimal except at the periphery. Scatter, on the other hand, contributes to the image near the structure which gave rise to it, and, therefore, has a much stronger influence on image contrast.

Tomographic resolution

Line sources of ^{99m}Tc and ^{123}I reconstructed with and without an apodization window were compared for the

two collimators (Tables 2 and 3). To compare the performance of the collimators under different imaging conditions we used the autocorrelation width calculated from unwindowed reconstructions.

The resolution of the LB collimator was superior to that of the LEGP under all conditions. For ^{99m}Tc, the ratio of the ACW of the LB to that of the LEGP at a radius of rotation of 17 cm was 1:1.32 ± 0.09; at 22 cm it was 1:1.41 ± 0.08. The ratios for ^{123}I were 1:1.53 ± 0.15 and 1:1.59 ± 0.11, respectively.

The resolution of the LB collimator was less dependent on radius of rotation than was that of the LEGP. The ratio of ACWs for imaging ^{99m}Tc at 17 cm compared with a 22 cm radius of rotation was 1:1.10 ± 0.07 for the LB and 1:1.18 ± 0.08 for the LEGP. For ^{123}I, the ratios were 1:1.13 ± 0.4 for the LB and 1:1.17 ± 0.09 for the LEGP.

For clinical brain imaging, however, the LB collimator can be used at 17 cm radius of rotation, while the LEGP, for our system, requires 22 cm to clear the patients' shoulders. For this situation, the ratio of the ACW of the LB at 17 cm to that of the LEGP at 22 cm was 1:1.56 ± 0.11 for ^{99m}Tc and 1:1.79 ± 0.16 for ^{123}I.

The loss in resolution due to the presence of high-energy photons from (p, 2n) ^{123}I was less for the LB than for the LEGP. The ratios describing the resolution degradation using ^{123}I compared with ^{99m}Tc were 1:1.06 ± 0.10 for the LB at a 17 cm radius of rotation and 1:1.09 ± 0.07 at 22 cm; for the LEGP, the corresponding ratios were 1:1.23 ± 0.10 and 1:1.23 ± 0.08.

The tomographic MTFs for ^{99m}Tc and ^{123}I are shown in Fig. 3. For both isotopes, the LB collimator response fell off more slowly at medium and high spatial frequencies than did the LEGP response. For ^{123}I, the MTFs fall off more rapidly between 0 and 0.1 cm^{-1}. This is caused by the low spatial frequency components due to increased penetration and scatter and is more prominent for the LEAP. The irregularities in the high-frequency portion of the ^{123}I MTFs were caused by low counting statistics resulting from the lower specific activity of ^{123}I in the line source and by truncation of the LSF at the edge of the field-of-view.

The same measurements were repeated using the Hanning apodization window with a cutoff frequency of 0.8 cm^{-1} (Tables 2 and 3). All ratios confirm the better overall response of the LB.

The spatial resolution for ^{99m}Tc at a 17 cm radius of rotation was the same for the LB using a windowed reconstruction and the LEGP without apodization (ACW 3.03 ± 0.08 compared with 3.06 ± 0.14 cm). For ^{123}I there is a clear advantage of the LB over the LEGP (3.16 ± 0.03 compared with 3.76 ± 0.24 cm). The LB at 17 cm radius of rotation with a windowed reconstruction outperformed the LEGP at 22 cm without an apodization window; the resolution ratio of ^{99m}Tc was 1:1.19 ± 0.06 and 1:1.40 ± 0.06 for ^{123}I.

Tc-99m   I-123(p,2n)

LB(17cm)
LB(22cm)
LEGP(17cm)
LEGP(22cm)

LB(17cm)
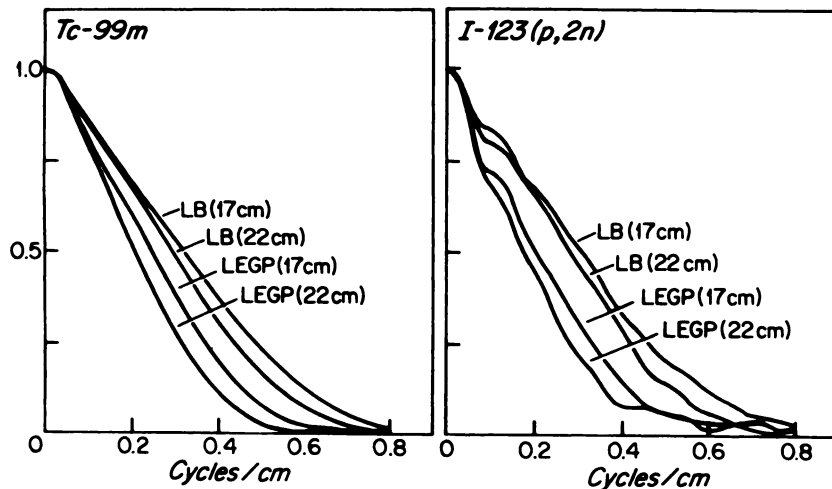LB(22cm)
LEGP(17cm)
LEGP(22cm)

Cycles/cm   Cycles/cm

FIGURE 3

^{99m}Tc and ^{123}I line sources in center of cylindrical 20-cm-diameter, water-filled phantom were imaged tomographically (128 projections over 360°). Resultant MTF are displayed for both long-bore (LB) and general-purpose (LEGP) collimator. Radii of rotation of 17 cm and 22 cm are given with respect to outer collimator surface. LB collimator maintains higher responses at all spatial frequencies

Noise measurements

The measured %RMS noise in acquisitions of 30 and 40 sec per projection using the Hanning windowed backprojection were 5.6% and 5.5% for the LEGP and 8.6% and 7.4% for the LB. These measurements correspond to the acquisition mode currently used for clinical imaging of [^{123}I]IMP brain studies. The noise amplification constants (k), which describe the image noise as a function of total counts, are reported in Table 4. Applying the Hanning window with 0.8 cm^{-1} cutoff frequency resulted in a decrease in k by almost a factor of 3 compared to the unwindowed reconstruction. The introduction of additional filtering between slices with the same filter kernel resulted in a more isotropic point response because the same filter was now applied to all three dimensions. While the resolution within the slice was not affected, this filter reduced k by a factor of 4 compared to the unwindowed reconstruction. The measured %RMS noise in the same datasets used above was 3.8 and 3.6% for the LEGP and 5.6 and 4.5% for the LB collimator (Fig. 4).

Patient studies

Reconstructed images from the [^{123}I]IMP brain studies contained more detail with an improved gray-to-white-matter contrast using the LB collimator (Fig. 5). All observers agreed that the LB images were superior and that the slightly increased "mottle" due to the increased noise level was not a significant disadvantage. The improved contrast of small structures, however, made possible detection of small lesions such as an internal capsule infarction (Fig. 6).

Geometric calculations

The results of our calculations for the LEGP and LB collimator and the low-energy, high resolution (LEHR) and medium-energy (ME) collimator are shown in Table 1. The ME collimator was the most efficient, but its poor resolution led to the lowest image contrast for the lesions we considered (0.5–3 cm diameter). The LEHR

had the best resolution of all four collimators, and provided the highest image contrast. The data in Table 1 demonstrate the overwhelming importance of resolution for imaging small objects. The 4% improvement in resolution of the LEHR over the LB yielded an 11% improvement in contrast for the 0.5 cm diameter lesion.

On our present system, the LEHR and the LEGP collimators can be used only at a radius of rotation of 22 cm with FWHM resolution of 1.29 and 1.72 cm; the resolution of the LEHR is worse than that of the LB collimator with a FWHM of 1.15 cm at its operating distance of 18 cm. A cutoff camera head with a radius of rotation of 13 cm for both the LEGP and the LEHR (35) would result in an increase in the FWHM resolution to 1.18 cm for the LEGP and to 0.90 cm for the LEHR collimator.
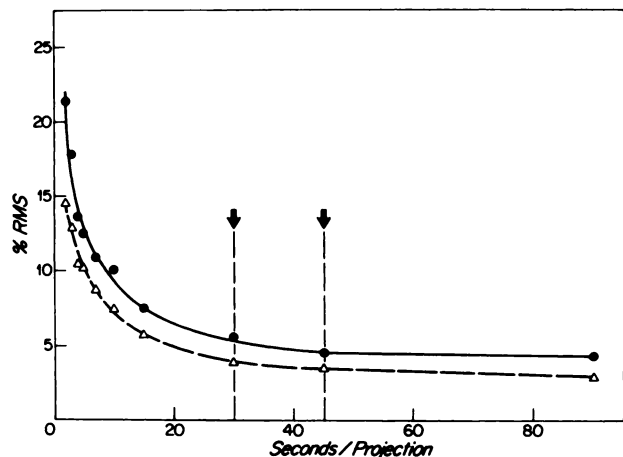

FIGURE 4

%RMS image noise in 20-cm-diameter cylindrical phantom (^{123}I at 1 µCi/ml specific activity), reconstructed with three-dimensional Hanning apodization window (cutoff 0.8 cm^{-1}) is displayed as function of acquisition time. Although sensitivity of collimator is lower than that of LEGP by factor of 0.32, %RMS noise is only slightly higher. Two vertical lines mark range of typical clinical acquisition times (△—△) LEAP; (●—●) Long bore
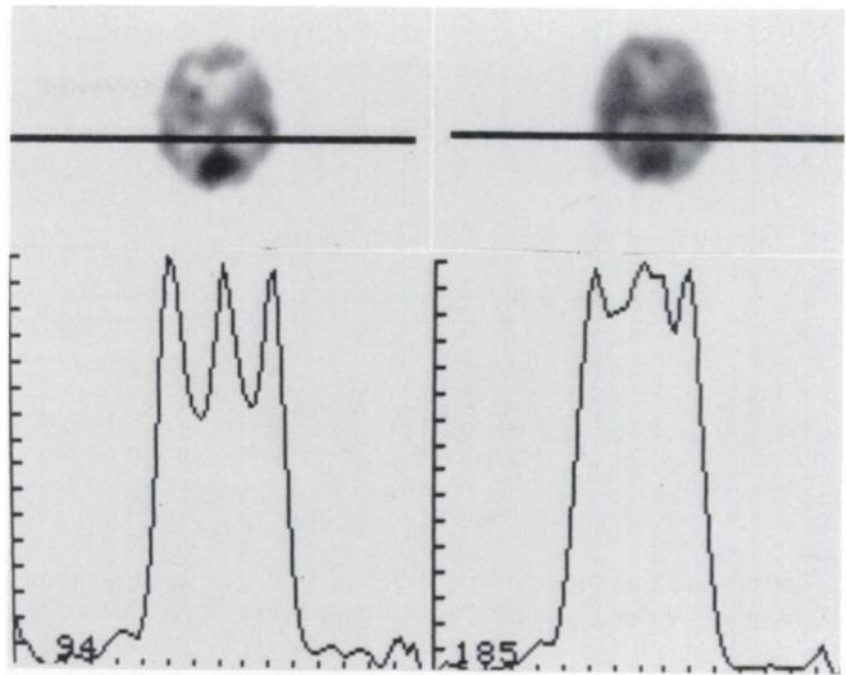
FIGURE 5
Comparison of same anatomic slice of IMP scans with LB and LEGP collimators obtained in same patient (64 × 64 matrix, 64 projection, 40 sec/projection, three-dimensional Hanning window). Improved contrast in LB image outweighs slightly increased noise compared with LEAP collimator

DISCUSSION

In this study, we showed that the improved resolution of the LB collimator compared to the LEGP collimator becomes increasingly important as the size of the object decreases, and outweighs the loss in sensitivity when small objects are imaged. These results were confirmed by clinical brain imaging, in which small structures such as the cortex (4 mm) and basal ganglia (1.5 cm) were more sharply defined on the LB images, although
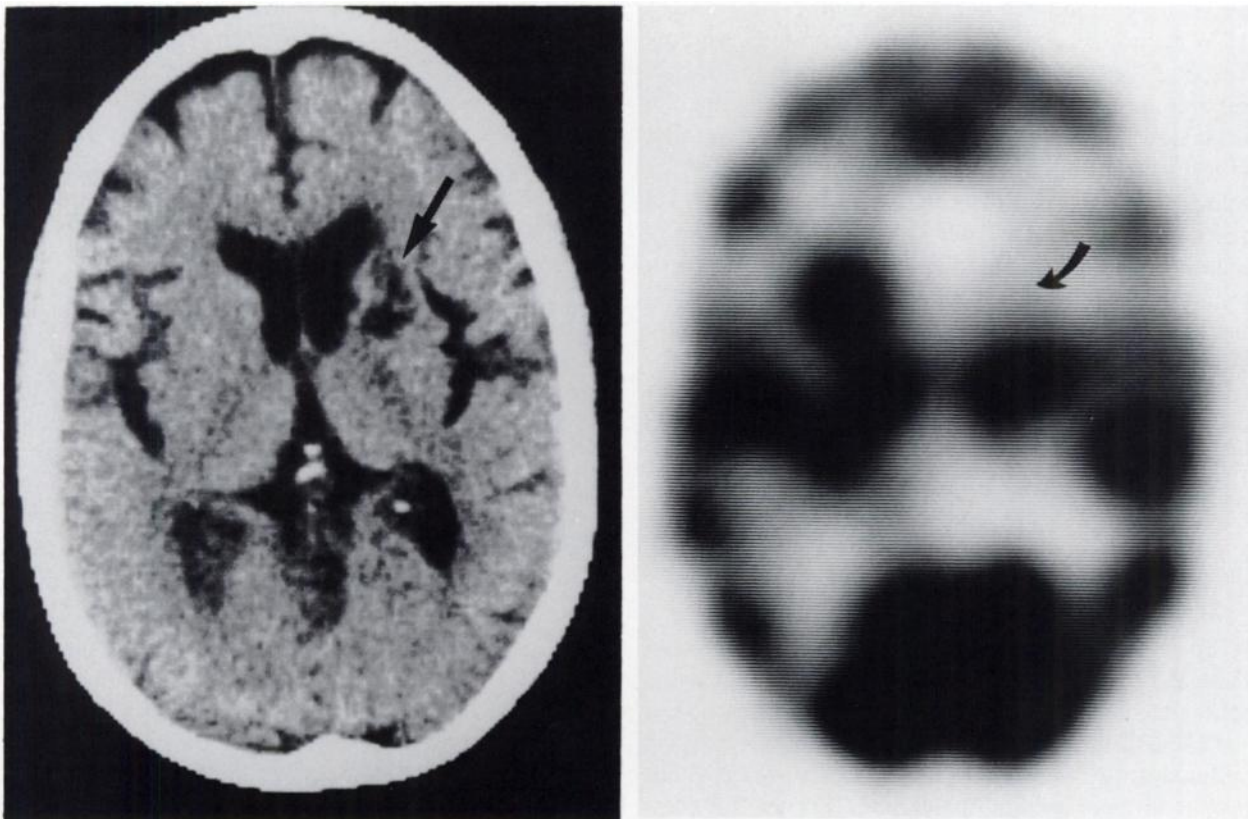

FIGURE 6
Patient with caudate nucleus infarct (CT scan on left; black arrow). Iodine-123 IMP SPECT using long-bore collimator shows corresponding perfusion defect (curved arrow)

the %RMS noise for the LB was 1.7 times that of the LEGP collimator. A similar conclusion was reached when a low-energy, general-purpose collimator was compared to a medium-energy collimator (9). The higher contrast of the LEGP collimator for small structures resulting from better spatial resolution outweighed the contrast degradation due to higher collimator penetration. These results are not surprising. A higher-resolution system is capable of transmitting more high-frequency information; this improves image contrast and becomes increasingly important for object detection as the object size decreases (Table 1). When higher-order tasks, such as localization and identification of cortical and ganglional structures and the recognition of abnormalities in shape, size, or uptake are considered, the improved resolution outweighs losses in sensitivity (20,21).

For imaging systems in general, MTFs and noise-power spectra cannot be described by simple mathematical expressions, and the analytic formulation of the task-specific SNR (the ideal figure of merit) remains an intractable problem. Therefore, we adopted a simplified approach by comparing systems at equal bandwidth (resolution). Equivalent resolution was achieved by choosing appropriate apodization windows, thereby degrading the LB resolution to that of the LEGP. We then compared the %RMS noise passed through the system for stationary noise in a uniform source. At 3.03 cm ACW for the LB collimator with a Hanning window (0.8 cm⁻¹ cutoff) and 3.06 cm ACW for the LEGP without apodization window, the %RMS noise for the LB was reduced by a factor of 3.0 for the same number of counts. This is equivalent to increasing sensitivity by a factor of 9.0. The measured sensitivity of the LB collimator is 0.32 times that of the LEGP (33). Therefore, there was an overall gain of a factor of 2.9 in resolution equivalent sensitivity for imaging ^{99m}Tc.

Our results can be explained in terms of aperture theory (12,13). For a large, uniform source, the variance, or total noise power, in a projection is given by the mean number of counts in a pixel and is, therefore, dependent on collimator sensitivity. The shape of the noise-power spectrum is not affected by collimator resolution, since each measured projection value is independent of all others. For the same apodization window we found the same noise amplification constant (k) for both collimators. The noise was sampled up to the Nyquist frequency of 0.8 cm⁻¹, which was also found to be the highest signal frequency present when a line source at the center of the phantom was imaged. For the LEGP collimator, the signal is bandlimited by the collimator; the white projection noise, however, is not subject to any bandlimiting process. For the LB collimator, the signal is bandlimited to a lesser degree (higher resolution) by the collimator. When a second low-pass filter, the apodization window, was applied,

the overall signal bandwidth (3.03 cm ACW) was the same. This apodization window not only attenuates high signal frequencies, it also bandlimits the noise and reduces the total noise power, or variance, in the image.

A resolution improvement over the LEGP could be achieved at a lower cost in sensitivity by building a thinner collimator, such as the LEHR. Furthermore, for a given collimator design a substantial improvement in resolution without sacrifice in efficiency is possible by reducing the imaging distance by using a slant hole collimator (10,34), or a modified "cutoff" camera head (35).

A second factor contributing to the superior image quality of the LB collimator is its lower penetration compared with the LEGP. Most of the resolution degradation due to high-energy photons arises from scatter of penetrating high-energy photons in the crystal, rather than from scatter in the patient (8). Because of the poor stopping power of low- and medium-energy collimators for primary photons with energies of 500 keV or higher, the penetration response is essentially a source-independent uniform background (5). As seen from our simulations, the effect of this constant background on the image contrast in the reconstructed image is minimal. This is consistent with the results of Polak et al. (10). The contribution from scatter, on the contrary, adds object dependent long tails to the reconstructed image; these degrade the image contrast. This scatter component is increased in the presence of high-energy photons from ^{123}I/^{124}I. Therefore, for tomographic imaging, we consider the rejection of high-energy photons which have been scattered in the patient more significant than primary penetration. Lower penetration can be achieved at lower cost in efficiency with a thinner collimator with thicker septa, such as the LEHR. The LB collimator, although a substantial improvement over the LEGP, is not optimal.

Our geometric collimator calculations allow us to assess collimators which were not evaluated in the experimental part of our study. Of all commercially available collimators considered, the LEHR collimator is the most suitable for brain SPECT. Its resolution is slightly better than that of the LB, resulting in improved image contrast for small lesions. Its 45% higher efficiency can be expected to lead to a 21% increase in %RMS noise for the same scan time. Furthermore, its lower penetration implies improved image quality for scans using ^{123}I.

Contrast ratios at different distances cannot be quantitatively be predicted because the penetration fraction is distance-dependent. A detailed analysis of the tradeoffs between resolution, sensitivity, and penetration is beyond the scope of this study; such a study could be addressed by Monte Carlo simulation or ray-tracing techniques. Qualitatively, however, it can be argued that the penetration fraction would be increased at the

closer imaging distances possible with a cutoff head or slant-hole collimator. The low penetration of a collimator design such as the LEHR should, therefore, be an additional advantage over the LEGP at the smaller radius of rotation. This suggests that commercially available collimators with characteristics similar to LEHR are better suited for SPECT brain imaging with a rotating gamma camera.

We have shown that the LB collimator provides better contrast of small structures than does the LEGP collimator. Observer performance in higher-order imaging tasks is known to improve with increasing contrast for small structures, even at the cost of sensitivity. Brain SPECT imaging involves higher-order imaging tasks; therefore, observer performance will increase with improved resolution, and, consequently, improved contrast for small structures. High resolution should be obtained by using a high-resolution collimator and a "smoother" reconstruction filter, rather than a more sensitive lower-resolution collimator and a "sharper" filter. Collimators should, therefore, be designed to provide high resolution, even at the cost of sensitivity.

FOOTNOTES

* General Electric Medical Systems, Milwaukee, WI.
† General Electric Medical Systems, Milwaukee, WI (General Electric 400 AT).
‡ Medi-Physics, Inc., Richmond, CA.

ACKNOWLEDGMENTS

REFERENCES

1. Holman BL, Hill TC, Magistretti PL: Brain imaging with emission computed tomography and radiolabeled amines. *Invest Radiol* 17:206-215, 1982
2. Hill TC, Holman BL: Cerebral perfusion imaging. In *Yearbook of Nuclear Medicine*, Hoffer PB, Gottschalk A, Zaret BL, eds. Chicago, Yearbook Medical Publishers, 1984, pp 13-23
3. Johnson KA, Mueller SP, Walshe TM, et al: Cerebral perfusion imaging in Alzheimer's disease with SPECT and I-123 IMP. *Neurology* (Suppl 1):35 235, 1985
4. Baker GA, Lum DJ, Smith EM, et al: Significance of radiocontaminants in I-123 for dosimetry and scintillation camera imaging. *J Nucl Med* 17:740-743, 1976
5. Bolmsjo MS, Persson BRR, Strand SE: Imaging I-123 with a scintillation camera. A study of detection performance and quality factor concepts. *Phys Med Biol* 22:266-277, 1977
6. Coleman RE, Greer KL, Drayer BP, et al: Collimation for I-123 imaging with SPECT. In *Emission Computed Tomography: Current Trends*, Esser PD, ed. New York, The Society of Nuclear Medicine, 1983, pp 135-145

7. Graham LS, Zielinski FW: Scintillation camera imaging with I-123. *Radiology* 130:519-523, 1979
8. McKeighen RE, Muehllehner G, Moyer RA: Gamma camera collimator considerations for imaging I-123. *J Nucl Med* 15:328-331, 1974
9. Polak JF, English RJ, Holman BL: Performance of collimators used for tomographic imaging of I-123 contaminated with I-124. *J Nucl Med* 24:1065-1069, 1983
10. Polak JF, Holman BL, Moretti J-L, et al: I-123 HIPDM brain imaging with a rotating gamma camera and slant-hole collimator. *J Nucl Med* 25:495-498, 1984
11. Hanson KM: Detectability in computed tomographic images. *Med Phys* 6:441-451, 1979
12. Wagner RF: Decision theory and the detail signal-to-noise ratio of Otto Schade. *Phot Sci Eng* 22:41-46, 1978
13. Wagner RF, Brown DG, Pastel MS: Application of information theory to the assessment of computed tomography. *Med Phys* 6:83-94, 1979
14. Budinger TF, Derenzo SE, Greenberg WL, et al: Quantitative potentials of dynamic emission computed tomography. *J Nucl Med* 19:309-315, 1978
15. Huesman RH: Analysis of statistical errors for transverse section reconstruction. *Lawrence Berkeley Lab Rep* LBL-4278, 1975
16. Shepp LA, Logan BF: The Fourier reconstruction of a head section. *IEEE Trans Nucl Sci* NS-21:21-43, 1974
17. Mazziotta JC, Phelps ME, Plummer D, et al: Quantitation in positron emission computed tomography: 5. Physical-anatomical effects. *J Comput Assist Tomogr* 5:734-743, 1981
18. Hoffman EJ, Huang SC, Phelps ME: Quantitation in positron emission computed tomography: 1. Effect of object size. *J Comput Assist Tomogr* 3:299-308, 1979
19. Kessler RM, Ellis JR, Murray E: Analysis of emission tomographic scan data: Limitations imposed by resolution and background. *J Comput Assist Tomogr* 8:514-522, 1984
20. Hanson KM: Variations in task and the ideal observer. *Proc SPIE* 419:60-67, 1983
21. Muehllehner G: Effect of resolution improvement on required count density in ECT imaging: A computed simulation. *Phys Med Biol* 30:163-173, 1985
22. Phelps ME, Huang SC, Hoffman EJ, et al: An analysis of signal amplification using small detectors in positron emission tomography. *J Comput Assist Tomogr* 6:551-565, 1982
23. Palmer DW, Knobel JW, Collier BD, et al: Collimator for emission tomography of the head. *Radiology* 149:231, 1983
24. Bracewell R: *The Fourier Transform and Its Applications*, New York, McGraw Hill, 1978
25. Beck RN, Zimmer LT, Charleston DB, et al: Advances in fundamental aspects of imaging systems and techniques. In *Medical Radioisotope Scintigraphy*, International Atomic Energy Agency SM-164/301:3-43, 1972
26. Knoop BO, Jordan K, Judas R, et al: Spatial resolution in imaging systems: Equivalent width—a realistic measure to replace FWHM. *J Nucl Med* 25:P22, 1984 (abstr)
27. Anger HO: Radioisotope cameras. In *Instrumentation in Nuclear Medicine*, Hine GH, ed. New York, Academic Press, 1964, pp 485-552

28. Gerber MS, Miller DW: Parallel-hole collimator design. *J Nucl Med* 15:724–725, 1970

29. Axelsson B, Msaki P, Isrealsson A: Subtraction of Compton scattered photons in single-photon emission computerized tomography. *J Nucl Med* 25:490–494, 1984

30. Floyd CE, Jaszczak RJ, Greer KL, et al: Deconvolution of Compton scatter in SPECT. *J Nucl Med* 26:403–408, 1985

31. English RJ, Polak JF, Holman BL: An iterative method for verifying systematic nonuniformities in refillable flood sources. *J Nucl Med Technol* 12:7–9, 1984

32. Sorenson JA, Cameron JR: *Instrumentation in Nuclear Medicine*, New York, Academic Press, 1974

33. Mueller St, Polak JF, Holman BL, et al: SPECT imaging with the long bore collimator: Loss in sensitivity vs. improved contrast resolution. *J Nucl Med* 25:P106, 1984 (abstr)

34. Esser PD, Alderson PO, Mitnick RJ, et al: Angled-collimator SPECT (A-SPECT): An improved approach to cranial single photon emission tomography. *J Nucl Med* 25:805–809, 1984

35. Larssen SA, Bergstrand G, Bergstedt H, et al: A special cut-off gamma camera for high-resolution SPECT of the head. *J Nucl Med* 25:1023–1030, 1984